Temperatures from Energy Balance Models: the effective heat capacity matters

Gerrit Lohmann[1,2]

[1]Alfred Wegener Institute, Helmholtz Centre for Polar and Marine Research, Bremerhaven, Germany
[2] University of Bremen, Bremen, Germany

Correspondence: Gerrit Lohmann (Gerrit.Lohmann@awi.de)

Abstract. Energy balance models (EBM) are highly simplified systems of the climate system. The global temperature is calculated by the radiation budget through the incoming energy from the Sun and the outgoing energy from the Earth. The argument that the temperature can be calculated by the simple radiation budget is revisited. The underlying assumption for a realistic temperature distribution is explored: One has to assume a moderate diurnal cycle due to the large heat capacity and the fast rotation of the Earth. Interestingly, the global mean in the revised EBM is very close to the originally proposed value. A linearized EBM implicitly assumes the heat capacity and the fast rotation arguments. The main point is, that the effective heat capacity and its temporal variation over the daily/seasonal cycle needs to be taken into account when estimating surface temperature from the energy budget. The time dependent-EBM predicts a flat meridional temperature gradient for large heat capacities. Motivated by this finding, a sensitivity experiment with a complex model is performed where the vertical diffusion in the ocean has been increased. The resulting flat meridional temperature gradient and reduced seasonal cycle is also found in climate reconstructions, suggesting a possible mechanism for past climate changes prior to 3 million years ago.

Keywords. Energy balance model, Earth system modeling, Temperature gradient, Climate change, Climate sensitivity, Climate reconstructions

1 Introduction

Energy balance models (EBMs) are among the simplest climate models. They were introduced almost simultaneously by Budyko (1969) and Sellers (1969). Because of their simplicity, these models are easy to understand and facilitate both analytical and numerical studies of climate sensitivity (Peixoto and Oort, 1992; Hartmann, 1994; Saltzmann, 2001; Ruddiman, 2001; Pierrehumbert, 2010). A key feature of these models is that they eliminate the climate's dependence on the wind field, ocean currents, the Earth rotation, and thus have only one dependent variable: the Earth's near-surface air temperature T.

With the development of computer capacities, simpler models have not disappeared; on the contrary, a stronger emphasis has been given to the concept of a hierarchy of models' as the only way to provide a linkage between theoretical understanding and the complexity of realistic models (von Storch et al. 1999; Claussen et al. 2002). In contrast, many important scientific debates in recent years have had their origin in the use of conceptually simple models (Le Treut et al., 2007; Stocker, 2011), also as a way to analyze data (Köhler et al., 2010) or complex models (Knorr et al., 2011).

Pioneering work has been done by North (North, 1975a, b; 1981; 1983) and these models were applied subsequently (e.g., Ghil, 1976; Su and Hsieh, 1976; Ghil and Childress, 1987; Short et al., 1991; Stocker et al., 1992; North and Kim, 2017). Later the EMBs were equipped by the hydrological cycle (Chen et al., 1995; Lohmann et al., 1996; Fanning and Weaver ,1996; Lohmann and Gerdes, 1998) to study the feedbacks in the atmosphere-ocean-sea ice system. One of the most useful examples of a simple, but powerful, model is the one-/zero-dimensional energy balance model. As a starting point, a zero-dimensional model of the radiative equilibrium of the Earth is introduced (Fig. 1)

$$(1-\alpha)S\pi R^2 = 4\pi R^2 \epsilon\sigma T^4 \tag{1}$$

where the left hand side represents the incoming energy from the Sun (size of the disk= shadow area πR^2) while the right hand side represents the outgoing energy from the Earth (Fig. 1). T is calculated from the Stefan-Boltzmann law assuming a constant radiative temperature, S is the solar constant - the incoming solar radiation per unit area– about $1367\,\mathrm{Wm}^{-2}$, α is the Earth's average planetary albedo, measured to be 0.3. R is Earth's radius $= 6.371 \cdot 10^6$ m, σ is the Stefan-Boltzmann constant $= 5.67 \cdot 10^{-8} \mathrm{JK}^{-4}\mathrm{m}^{-2}\mathrm{s}^{-1}$, and ϵ is the effective emissivity of Earth (about 0.612) (e.g., Archer 2010). The geometrical constant πR^2 can be factored out, giving

$$(1-\alpha)S = 4\epsilon\sigma T^4 \tag{2}$$

Solving for the temperature,

$$T = \sqrt[4]{\frac{(1-\alpha)S}{4\epsilon\sigma}} \tag{3}$$

Since the use of the effective emissivity ϵ in (1) already accounts for the greenhouse effect we gain an average Earth temperature of 288 K ($15°$C), very close to the global temperature observations/reconstructions (Hansen et al., 2011) at $14°$C for 1951-1980. Interestingly, (3) does not contain parameters like the heat capacity of the planet. We will explore that this is essential for the temperature of the Earth's climate system.

Schwartz (2007) stressed out that the effective heat capacity is not an intrinsic property of the climate system but is reflective of the rate of penetration of heat energy into the ocean in response to the particular pattern of forcing and background state. We will evaluate the effect of the effective heat capacity in the climate system. Wang et al. (2019) showed a pronounced low equator-to-pole gradient in the annual mean sea surface temperatures is found in a numerical experiment conducted with a coupled model consisting of an atmospheric general circulation model coupled to a slab ocean model in which the mixed-layer thickness is reduced. In the present paper, it is shown that the heat capacity is linked to the long-lasting question of a low equator-to-pole gradients during the Paleogene/Neogene climate (Markwick, 1994; Wolfe, 1994; Sloan and Rea, 1996; Huber et al., 2000; Shellito et al., 2003; Tripati et al., 2003; Mosbrugger et al., 2005). Those published temperature patterns resemble the high latitude warming (with moderate low latitude warming) and reduced seasonality.

2 A closer look onto the spatial distribution

Let us have a closer look onto (1) and consider local radiative equilibrium of the Earth at each point. Fig. 2 shows the latittude-longitude dependence of the incoming short wave radiation. The global mean temperatures are not affected by the tilt (Berger and Loutre 1991; 1997; Laepple and Lohmann 2009). We assume an idealized geometry of the Earth, no obliquity and no precession, which makes an analytical calculation possible. Furthermore ϵ and α are assumed to be constants.

The incoming radiation goes with the cosine of latitude φ and longitude Θ, and there is only sunshine during the day. Fig. 2a shows the latitudinal dependence. As we assume no tilt (this assumption is later relaxed), the latitudinal dependence is a function of latitude only: $\cos\varphi$. On the right-hand side, the function is shown. Fig. 2b shows the latitudinal dependence is a function of longitude: $\cos\Theta$ for the sun-shining side of the Earth, and for the dark side of the Earth it is zero. For simplicity, we can define the angle Θ anti-clockwise on the for the sun-shining side between $-\pi/2$ and $\pi/2$. We define the maximal insolation always at $\Theta = 0$ which is moving in time. In the panel, the Earth's rotation is schematically sketched as the red arrow, and we see the time-dependence in the right-hand side. It is noted that the geographical longitude can be calculated by $mod(\Theta - 2\pi \cdot t/24, 2\pi)$ where t is measured in hours and mod is the modulo operation. Summarizing our geometrical considerations, we can now write the local energy balance as

$$\epsilon\sigma T^4 = (1-\alpha)S \cdot \cos\varphi \cdot \cos\Theta \qquad \text{for } -\pi/2 < \Theta < \pi/2.$$

$$= 0 \qquad \text{for} \quad \Theta < -\pi/2 \quad \text{or} \quad \Theta > \pi/2 \tag{4}$$

Temperatures based on the local energy balance without a heat capacity would vary between $T_{min} = 0$ K and $T_{max} = \sqrt[4]{\frac{(1-\alpha)S}{\epsilon\sigma}} = \sqrt{2} \cdot \sqrt[4]{\frac{(1-\alpha)S}{4\epsilon\sigma}} = \sqrt{2} \cdot 288K = 407$ K.

Integration of (4) over the Earth surface is

$$\int_{-\pi/2}^{\pi/2} \left(\int_0^{2\pi} \epsilon\sigma T^4 R\cos\varphi d\Theta \right) Rd\varphi = (1-\alpha)S \int_{-\pi/2}^{\pi/2} R\cos^2\varphi d\varphi \cdot \int_{-\pi/2}^{\pi/2} R\cos\Theta d\Theta$$

$$\epsilon\sigma R^2 \frac{4\pi}{4\pi} \int_{-\pi/2}^{\pi/2} \left(\int_0^{2\pi} T^4 \cos\varphi d\Theta \right) d\varphi = (1-\alpha)SR^2 \underbrace{\int_{-\pi/2}^{\pi/2} \cos^2\varphi \, d\varphi}_{\frac{\pi}{2}} \cdot \underbrace{\int_{-\pi/2}^{\pi/2} \cos\Theta \, d\Theta}_{2}$$

$$\epsilon\sigma 4\pi \overline{T^4} = (1-\alpha)S\,\pi \tag{5}$$

giving a similar formula as (3) with the definition for the average

$$\overline{T^4} = \frac{1}{4\pi} \int_{-\pi/2}^{\pi/2} d\varphi \int_0^{2\pi} \cos\varphi \quad d\Theta \quad T^4 \quad .$$

What we really want is the mean of the temperature $\overline{T}$. Therefore, we take the fourth root of (4):

$$T = \sqrt[4]{\frac{(1-\alpha)S\cos\varphi\cos\Theta}{\epsilon\sigma}} \qquad \text{for } -\pi/2 < \Theta < \pi/2 \tag{6}$$

and zero elsewhere. If we calculate the zonal mean of (6) by integration at the latitudinal cycles we have

$$
\begin{aligned}
T(\varphi) &= \frac{1}{2\pi} \int\limits_{-\pi/2}^{-\pi/2} \sqrt[4]{\frac{(1-\alpha)S\cos\varphi\cos\Theta}{\epsilon\sigma}}\,d\Theta \\
&= \underbrace{\frac{\sqrt{2}}{2\pi} \int\limits_{-\pi/2}^{\pi/2} (\cos\Theta)^{1/4}d\Theta}_{\sqrt{\pi}\Gamma(5/8)/\Gamma(9/8)} \quad \sqrt[4]{\frac{(1-\alpha)S}{4\epsilon\sigma}} \quad (\cos\varphi)^{1/4} \quad = \quad \underbrace{\frac{1}{\sqrt{2\pi}}\frac{\Gamma(5/8)}{\Gamma(9/8)}}_{\approx 0.608}\cdot\sqrt[4]{\frac{(1-\alpha)S}{4\epsilon\sigma}} \quad (\cos\varphi)^{1/4}
\end{aligned}
\tag{7}
$$

as a function on latitude (Fig. 3). Γ is Euler's Gamma function with $\Gamma(x+1) = x\Gamma(x)$. When we integrate this over the latitudes, we obtain

$$
\begin{aligned}
\overline{T} &= \frac{1}{2} \int\limits_{-\pi/2}^{\pi/2} T(\varphi)\cos\varphi\,d\varphi \quad = \quad \frac{1}{2}\frac{\Gamma(5/8)}{\sqrt{2\pi}\,\Gamma(9/8)}\cdot\sqrt[4]{\frac{(1-\alpha)S}{4\epsilon\sigma}} \quad \underbrace{\int\limits_{-\pi/2}^{\pi/2} (\cos\varphi)^{5/4}d\varphi}_{\sqrt{\pi}\Gamma(9/8)/\Gamma(13/8)} \\
&= \frac{1}{2}\frac{1}{\sqrt{2}}\frac{\Gamma(5/8)}{\Gamma(13/8)}\cdot\sqrt[4]{\frac{(1-\alpha)S}{4\epsilon\sigma}} = \underbrace{\frac{\sqrt{2}}{4}\frac{8}{5}}_{F=0.4\sqrt{2}}\cdot\sqrt[4]{\frac{(1-\alpha)S}{4\epsilon\sigma}}
\end{aligned}
\tag{8}
$$

Therefore, the mean temperature is a factor $F = 0.4\sqrt{2} \approx 0.566$ lower than 288 K as stated at (3) and would be $\overline{T} = 163$ K. The standard EBM in Fig. 1 has imprinted into our thoughts and lectures. We should therefore be careful and pinpoint the reasons for the failure. What happens here is that the heat capacity of the Earth is neglected and there is a strong non-linearity of the outgoing radiation.

3 The heat capacity and fast rotating body

The energy balance shall take the heat capacity into account:

$$
\begin{aligned}
C_p\partial_t T &= (1-\alpha)S\cdot\cos\varphi\cdot\cos\Theta \quad -\epsilon\sigma T^4 \qquad \text{for } -\pi/2 < \Theta < \pi/2 \\
&= \qquad\qquad\qquad\qquad\qquad -\epsilon\sigma T^4 \qquad \text{elesewhere}
\end{aligned}
\tag{9}
$$

with C_p representing the heat capacity multiplied with the depth of the atmosphere-ocean layer (C_p is in the order of $10^7 - 10^8\,JK^{-1}m^{-2}$). If we consider the zonal mean and averaged over the diurnal cycle, we can assume that the heat capacity is mainly given by the atmosphere and the uppermost ocean and soil. Observational evidence is that the diurnal variation of the ocean surface is in the order of 0.5-3 K with highest values at favorable conditions of high insolation and low winds (Stommel, 1969; Anderson et al., 1996; Kawai and Kawamura, 2002; Stuart-Menteth, et al. 2003; Ward, 2006). To simplify (9), the energy balance is integrated over the longitude and day, and assume that the variation due to the diurnal cycle is weak. With

$\tilde{T} = \frac{1}{2\pi} \int\limits_0^{2\pi} T\, d\Theta$, we find

$$C_p\, \partial_t \tilde{T} \quad = \quad (1-\alpha)S\cos\varphi \cdot \underbrace{\frac{1}{2\pi} \int\limits_{-\pi/2}^{\pi/2} \cos\Theta\, d\Theta}_{2} - \epsilon\sigma \underbrace{\frac{1}{2\pi} \int\limits_0^{2\pi} T^4\, d\Theta}_{\approx \tilde{T}^4} \quad = \quad (1-\alpha)\frac{S}{\pi}\cos\varphi - \epsilon\sigma\tilde{T}^4 \tag{10}$$

giving the equilibrium solution

$$\tilde{T}(\varphi) = \sqrt[4]{\frac{4}{\pi}} \cdot \sqrt[4]{\frac{(1-\alpha)S}{4\epsilon\sigma}} \quad (\cos\varphi)^{1/4} \tag{11}$$

5   shown in Fig. 3 as the red line. The global mean temperature is

$$\overline{\overline{T}} \quad = \quad \sqrt[4]{\frac{4}{\pi}} \cdot \sqrt[4]{\frac{(1-\alpha)S}{4\epsilon\sigma}} \quad \underbrace{\frac{1}{2} \int\limits_{-\pi/2}^{\pi/2} (\cos\varphi)^{5/4} d\varphi}_{\sqrt{\pi}\Gamma(9/8)/\Gamma(13/8)} \quad = \quad \underbrace{\sqrt{\frac{\pi}{2}} \frac{\Gamma(9/8)}{\Gamma(13/8)}}_{G\approx 0.989} \cdot \sqrt[4]{\frac{(1-\alpha)S}{4\epsilon\sigma}} \quad \approx \quad 285 \text{ K} \tag{12}$$

which is very similar to 288 K from (3), since the factor $G = \sqrt{\frac{\pi}{2}} \frac{\Gamma(9/8)}{\Gamma(13/8)}$ is close to 1.

    A numerical solution of (9) is shown as the brownish dashed line in Fig. 3 where the diurnal cycle has been explicitly taken into account and $C_p = C_p^a$ has been chosen as the atmospheric heat capacity

$$C_p^a = c_p p_s/g = 1004\, JK^{-1}kg^{-1} \cdot 10^5 Pa/(9.81 ms^{-2}) = 1.02 \cdot 10^7\, JK^{-1}m^{-2}$$

which is the specific heat at constant pressure c_p times the total mass p_s/g. p_s is the surface pressure and g the gravity. The global mean temperature $\overline{T}$ is 286 K, again close to 288 K.

10   Quite often the linearization the long wave radiation $\epsilon\sigma T^4$ is linearized in energy balance models. Indeed the linearization is performed around $0°C$ (North et al., 1975a, b; Chen et al., 1995; Lohmann and Gerdes, 1998; North and Kim, 2017) and is formulated as $A + B \cdot T'$ with T' being measured in $°C$. As the temperatures based on the local energy balance without a heat capacity would vary between $T_{min} = 0$ K and $T_{max} = \sqrt{2} \cdot 288K = 407$ K, a linearization would be not permitted. Therefore, the linearization implicitely assumes the above heat capacity and fast rotation arguments.

15   The effect of heat capacity is systematically analyzed in Fig. 4. The temperatures are relative insensitive for a wide range of C_p. We find a severe drop in temperatures for heat capacities below 0.01 of the atmospheric heat capacity C_p^a. Fig. 5 shows the temperature dependence for different values of C_p and the length of the day, indicating a pronounced temperature drop during night for low values of heat capacities and for (hypothetical) long days of 240 h instead of 24 h. We have chosen this feature for a particular latitude (here: 45^0N). The analysis shows that the effective heat capacity is of great importance for the

20   temperature, this depends on the atmospheric planetary boundary layer (how well-mixed with small gradients in the vertical) and the depth of the mixed layer in the ocean which will be analyzed later.

4   Meridional temperature gradients

Equation (10) shall be the starting point for further investigations. One can easily include the meridional heat transport by diffusion which has been previously used in one-dimensional EBMs (e.g. Adem, 1965; Sellers, 1969; Budyko, 1969; North, 1975a,b). In the following we will drop the tilde sign. Using a diffusion coefficient k, the meridional heat transport across a
5 latitude is $HT = -k\nabla T$. One can solve the EBM

$$C_p \partial_t T = -\nabla \cdot HT + (1-\alpha)\frac{S}{\pi}\cos\varphi - \epsilon\sigma T^4 \quad . \tag{13}$$

numerically. The boundary condition is that the HT at the poles vanish. The values of k are in the range of earlier studies (North, 1975a,b; Stocker et al., 1992; Chen et al., 1995; Lohmann et al., 1996). Fig. 6 shows the equilibrium solutions of (13) using different values of k (solid lines). The global mean temperature is not affected by the transport term because it depends
10 only of global net radiative fluxes, not internal redistribution. Formally, the integration with boundary condition with zero heat transport at the poles provides no effect (note that $\partial_y T = 0$ at the North and South Pole). The same is true if we introduce zonal transports because of the cyclic boundary condition in $\theta-$direction.

Until now, we assumed that the Earth's axis of rotation were vertical with respect to the path of its orbit around the Sun. Instead Earth's axis is tilted off vertical by about 23.5 degrees. As the Earth orbits the Sun, the tilt causes one hemisphere to
15 receive more direct sunlight and to have longer days. This is a redistribution of heat with more solar insolation at the poles and less at the equator (formally it could be associated to an enhanced meridional heat transport HT). The resulting temperature is shown as the dotted blue line in Fig. 6. A spatially constant temperature in (1) can be formally seen as a system with infinite diffusion coefficient $k \to \infty$ (black line in Fig. 6).

The global mean temperatures are not affected by the tilt and the values are identical to the one calculated in (12). This is
20 true even if we calculate the seasonal cycle (Berger and Loutre, 1991; 1997; Laepple and Lohmann, 2009). However, if we include non-linearities such as the ice-albedo feedback (α as a function of T), the global mean value is changing (Budyko, 1969; Sellers, 1969; North et al., 1975a, b), cf. the dashed blue line in Fig. 6. Such model can be improved by including an explicit spatial pattern with a seasonal cycle to study the long-term effects of climate to external forcing (Adem, 1981; North et al., 1983) or by adding noise mimicking the effect of short-term features on the long-term climate (Hasselmann, 1976; Lemke,
25 1977; Lohmann, 2018).

As a logical next step, let us now include an explicit seasonal cycle into the EBM:

$$C_p \partial_t T = -\nabla \cdot HT + (1-\alpha)S(\varphi,t) - \epsilon\sigma T^4 \quad . \tag{14}$$

with $S(\varphi,t)$ being calculated daily (Berger and Loutre, 1991; 1997). Eq. (14) is calculated numerically for fixed diffusion coefficient $k = 1.5 \cdot 10^6 m^2/s$ under present orbital conditions. Fig. 7 indicates that the temperature gradient is getting flatter
30 for large heat capacities. Furthermore, the mean temperature is affected by the choice of C_p. In the case of large heat capacity at high latitudes (for latitudes polewards of $\varphi = 50°$ mimicking large mixed layer depths) and moderate elsewhere, we observe strong warming at high latitudes with moderate warming at low latitudes (dashed curve). This again indicates that we cannot neglect the time-dependent left hand side in the energy balance equations, both for the diurnal (9) as well as the seasonal (14)

cycle for the temperature budget. In both considered cases, at strong diurnal or seasonal amplitude lowers the annual mean temperature.

Fig. 8 shows the seasonal amplitude for the C_p-scenarios as indicated by the blue and dashed black lines, respectively. The larger the seasonal contrast, the colder is the climate. Let us define here $\bar{\cdot}$ as the averaging over a time period (here the seasonal cycle), then $\overline{T^4} > \overline{T}^4$ which is consistent with Hölder's inequality (Rodgers, 1888; Hölder 1889; Hardy et al., 1934, Kuptsov, 2001). It is noted that this feature is missing in the linearized version $A + B \cdot T'$ of the outgoing radiation. We see the large variation in the seasonal cycle $\Delta T = T_{summer} - T_{winter}$ for the blue line in Fig. 8 as compared to the dashed line. A mean change in the net long wave radiation can be approximated by the mean of summer and winter values $\epsilon\sigma \cdot 0.5(T_{summer}^4 + T_{winter}^4)$, which is up to $10\,Wm^{-2}$ higher than $\epsilon\sigma \cdot (0.5 \cdot (T_{summer} + T_{winter}))^4$ if the seasonal cycle is damped as in the dashed line of Fig. 8. This implies that a lower seasonal cycle provides for a significant warming. If we would consider a linear model $A + B \cdot T'$ with T' being measured in $°C$ for the long-wave radiation, the differences between the blue and the dashed line would be much lower, due to the absence of the non-linearity in net long wave radiation change.

5 Meridional temperature gradient in a complex model

In the following, a complex circulation model is used where the seasonal cycle is reduced by enhanced vertical mixing in the ocean. To make a rough estimate of the involved mixed layer, one can see that the effective heat capacity of the ocean is time-scale dependent. A diffusive heat flux goes down the gradient of temperature and the convergence of this heat flux drives a ocean temperature tendency:

$$C_p^o \partial_t T = -\partial_z (k^o \partial_z T) \tag{15}$$

where $k_v = k^o/C_p^o$ is the oceanic vertical eddy diffusivity in $m^2\,s^{-1}$, and C_p^o the oceanic heat capacity relevant on the specific time scale. The vertical eddy diffusivity k_v can be estimated from climatological hydrographic data (Olbers et al., 1985; Munk and Wunsch, 1998) and varies roughly between 10^{-5} and $10^{-4}\,m^2\,s^{-1}$ depending on depth and region. A scale analysis of (15) yields a characteristic depth scale h_T through

$$\frac{\Delta T}{\Delta t} = k_v \frac{\Delta T}{h_T^2} \quad \longrightarrow h_T = \sqrt{k_v\,\Delta t} \tag{16}$$

For the diurnal cycle h_T is less that half a meter and the heat capacity generally less than that of the atmosphere. The seasonal mixed layer depth can be several hundred meters (e.g., de Boyer Montégut et al., 2004). As pointed out by Schwartz (2007), the effective heat capacity that reflects only that portion of the global heat capacity that is coupled to the perturbation on the timescale of the perturbation. In the context of global climate change induced by changes in atmospheric composition on the decade to century timescale the effective heat capacity is subject to change in heat content on such timescales.

In order to test the effective heat capacity/mixing hypothesis, we employ the coupled climate model COSMOS which was developed at the Max-Planck Institute for Meteorology in Hamburg (Jungclaus et al., 2000). The model contains explicit diurnal and seasonal cycles, it has no flux correction and has been successfully applied to test a variety of paleoclimate hypotheses, ranging from the Miocene climate (Knorr et al., 2011; Knorr and Lohmann, 2014; Stein et al., 2016), the Pliocene (Stepanek

and Lohmann, 2012) as well as glacial (Zhang et al., 2013; 2014) and interglacial climates (Wei and Lohmann, 2012; Lohmann et al., 2013; Pfeiffer and Lohmann, 2016).

In order to mimic the effect of a higher effective heat capacity and deepened mixed layer depth, the vertical mixing co-efficient is increased in the ocean, changing the values for the background vertical diffusivity (arbitrarily) by a factor of 25, providing a deeper thermocline. Qualitative similar results are obtained when using a smaller factor (not shown). The mixing has a background value plus a mixing process strongly influenced by the shears of the mean currents. Although observations give a range of values of k_v for the ocean interior, models use simplified physics and prescribe a constant background value. The model uses a classical vertical eddy viscosity and diffusion scheme (Pacanowski and Philander, 1981). Orbital parameters are fixed to the present condition.

Fig. 9 shows the anomalous near surface temperature for the new vertical mixing experiment relative to the control climate (Wei and Lohmann, 2012). Both simulations were run over 1000 years of integration in order to receive a quasi-equilibrium at the surface. The differences are related to the last 100 years of the simulation. In the vertical mixing experiment k_v was enhanced leading to more heat is taken up by the ocean producing equable climates with pronounced warming at polar latitudes (Fig. 9). Heat gained at the surface is diffused down the water column, and, compared to the control simulation, the wind-induced Ekman cells in the upper part of the oceans intensified and deepened. Furthermore, the model indicates that the respective winter signal of high-latitude warming is most pronounced (Fig. 9), decreasing the seasonality, suggesting a common signal of pronounced warming and weaker seasonality, a feature already seen in our EBM (Fig. 8).

Previous studies have noted that changing the ocean mixed layer depth impacts the climatological annual mean temperature (Schneider and Zhu, 1998; Qiao et al., 2004; Donohoe et al., 2014; Wang et al., 2019). The increased heat capacity of the mixed layer reduced the magnitude of the annual cycle affecting the surface winds and upwelling which may provide non-linear effects (Wang et al., 2019). For the past, a strong warming at high latitudes is reconstructed for the Pliocene, Miocene, Eocene periods (Markwick, 1994; Wolfe, 1994; Sloan and Rea, 1996; Huber et al., 2000; Shellito et al., 2003; Tripati et al., 2003; Mosbrugger et al., 2005; Utescher and Mosbrugger, 2007). It is a conundrum that the modelled high latitudes are not as warm as the reconstructions (e.g., Sloan and Rea, 1996; Huber et al., 2000; Mosbrugger et al., 2005; Knorr et al., 2011; Dowset et al., 2013). The low latitude warming is only moderate. Inspired by the EBM and GCM results, we may think of a climate system having a higher effective heat capacity producing a reduced seasonal cycle and flat temperature gradients. The changed vertical mixing coefficients are mimicking possible effects like weak tidal dissipation or abyssal stratification (e.g., Lambeck 1977; Green and Huber, 2013), but its explicit physics is not evaluated here. It might be that the more effective mixing provides an explanation that high latitudes were much warmer than present and more equable in that the summer-to-winter range of temperature was much reduced (Sloan and Barron, 1990, Valdes et al., 1996; Sloan et al., 2001; Spicer et al. 2004). Interestingly, it has been suggested that the tight link between ocean temperature and CO_2 formed only during the Pliocene when the thermocline shoals and surface water became more sensitive to CO_2 (La Riviere et al., 2012) which is therefore of major importance for the understanding of the climate-carbon cycle (Wiebe and Weaver, 1999; Zachos et al., 2008; de Boer and Hogg, 2014).

6   Conclusions

This manuscript revisits the relationship between the (global mean) surface temperature of the Earth and its radiation budget as is frequently used in Energy balance models (EBMs). The main point is, that the effective heat capacity and its temporal variation over the daily/seasonal cycle needs to be taken into account when estimating surface temperature from the energy budget. EMBs provide a crucial tool in climate research, especially because they - confirmed by the results of the elaborate realistic climate models - describe the processes essential for the genesis of the global climate. EBMs are thus an admissible conceptual tools, due to its reduced complexity to the essentials "scientific understanding" represents (von Storch et al., 1999). This understanding states that the radiation balance on the ground and the absorption in the atmosphere are the essential factors for determining the temperature. Eq. (3) says that the temperature is independent of the size of the Earth and the thermal characteristics, but depends on the albedo, emissivity and solar constant.

The argument follows the conservation of energy: in steady state the Earth has to emit as much energy as it receives from the Sun. However, I argue that we shall explicitly emphasize the Earth as a rapidly rotating object with a significant heat capacity in our EBMs. Without these effects, the global mean temperature would be much lower (in the order of 163 K). This description can be better used for objects like the Moon or Mercury (Vasavada et al., 1999) as slowly rotating bodies without significant heat capacity. The Earth system understanding says that these effects are important for the radiation balance, other processes - like horizontal transport processes or the ice-albedo feedback - are only of secondary importance for the globally averaged temperature. The linearization of the long wave radiation in several models (North et al., 1975a, b; Chen et al., 1995) implicitely assumes the above heat capacity and fast rotation arguments. Ironically, the global mean temperature in the revised EBM is very close to the original proposed value.

As a basic feature, we detect the strong dependence of the temperature distribution on the effective heat capacity linked to the mixed-layer depth. A change in the mixed layer depth which likely happened through glacial-interglacial cycles (e.g. Zhang et al., 2014) can therefore an important driver constraining climate sensitivity (Köhler, et al., 2010). This could be also relevant for future climate change when the ocean stratification can change. This is indeed emphasized in a sensitivity study of climatological SST to slab ocean model thickness (Wang et al., 2019). It is concluded that climate studies should use improved representations of vertical mixing processes including turbulence, tidal mixing, hurricanes and wave breaking (e.g., Qiao et al., 2004; Huber et al., 2004; Simmons et al., 2004; Korty et al., 2008; Griffiths and Peltier, 2009; Green and Huber, 2013; Reichl and Hallberg, 2018). Global climate models treat ocean vertical mixing as static, although there is little reason to suspect this is correct (e.g., see Munk and Wunsch, 1998). In numerical modelling, the values are also constrained by the required numerical stability and to fill gaps left by other parameterisations (e.g., Griffies, 2005). As a natural next step, one shall analyze the ocean mixing/heat uptake (Luyten et al., 1983; Large et al., 1994; Nilsson, 1995) to understand past, present and future temperatures.

Acknowledgements. Thanks go to Peter Köhler, Dirk Olbers, and anonymous referees for comments on earlier versions of the manuscript. Madlene Pfeiffer and Christian Stepanek are acknowledged for their contribution in producing Fig. 7. This work was funded by the Helmholtz Society through the research program PACES.
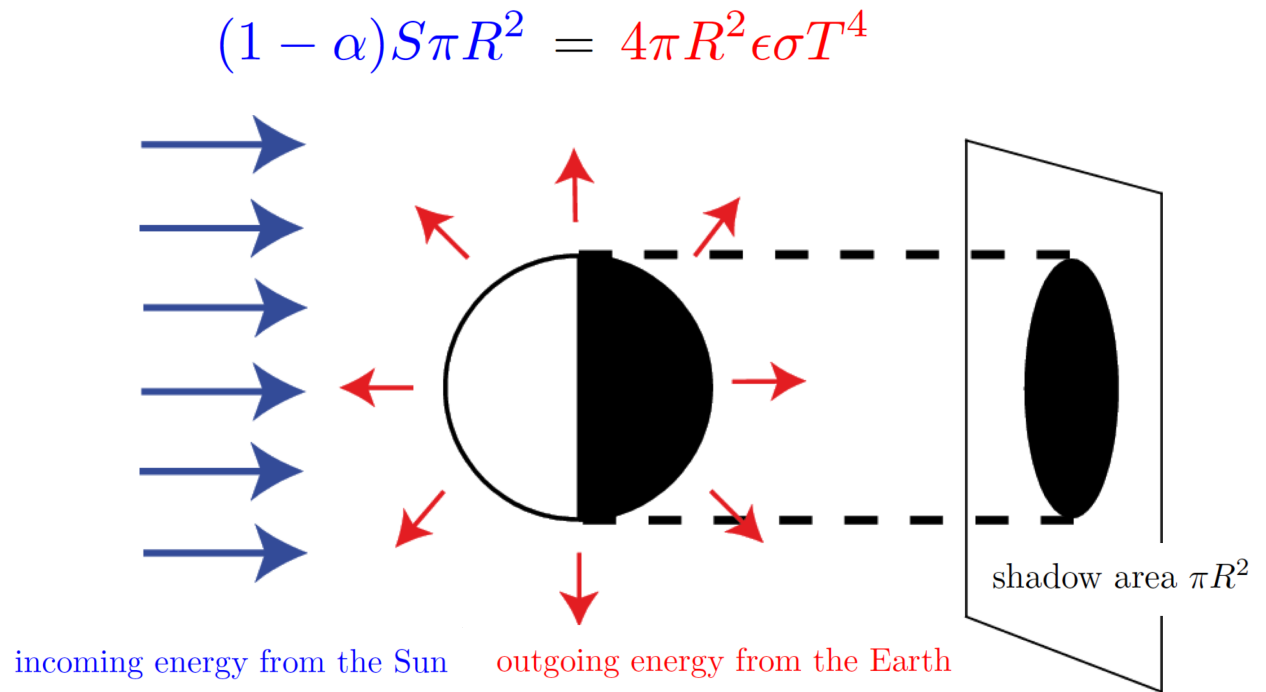
Figure 1. Schematic view of the energy absorbed and emitted by the Earth following (1). Modified after Goose (2015).
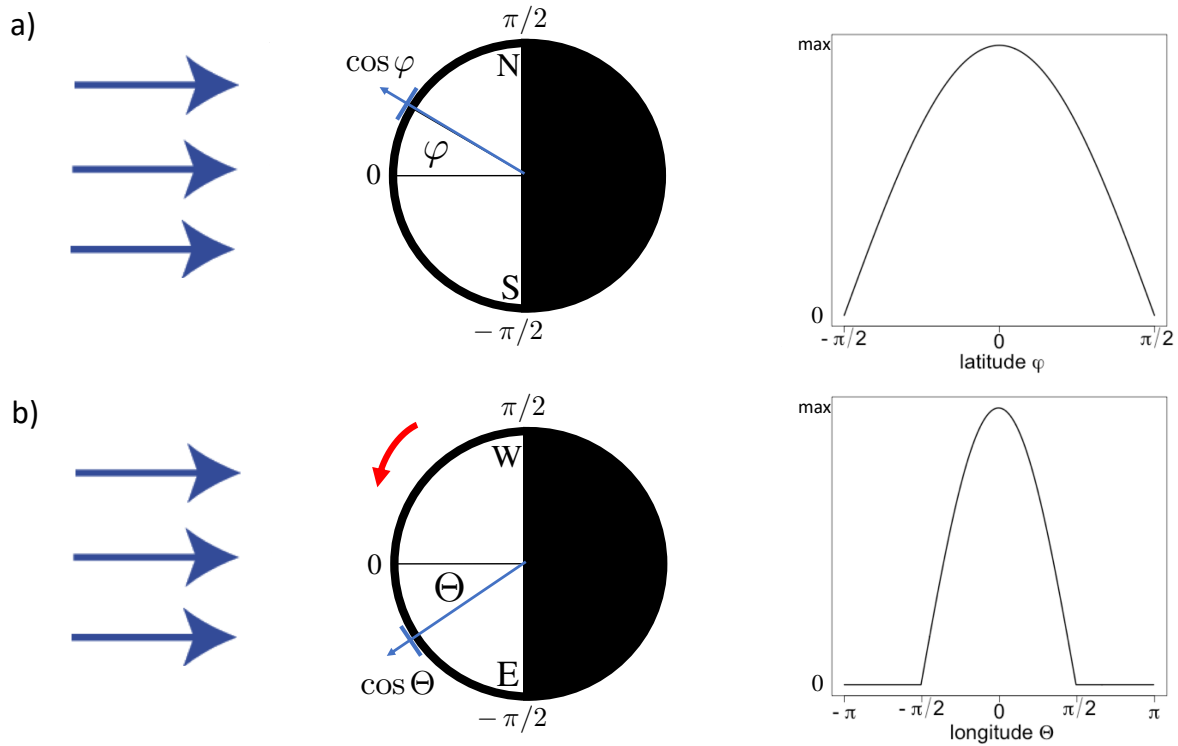
Figure 2. Latitudinal (a) and longitudinal (b) dependence of the incoming short wave radiation. On the right hand side, the insolation as a function of latitude φ and longitude Θ with maximum insolation $(1 - \alpha)S$ is shown. See text for the details.
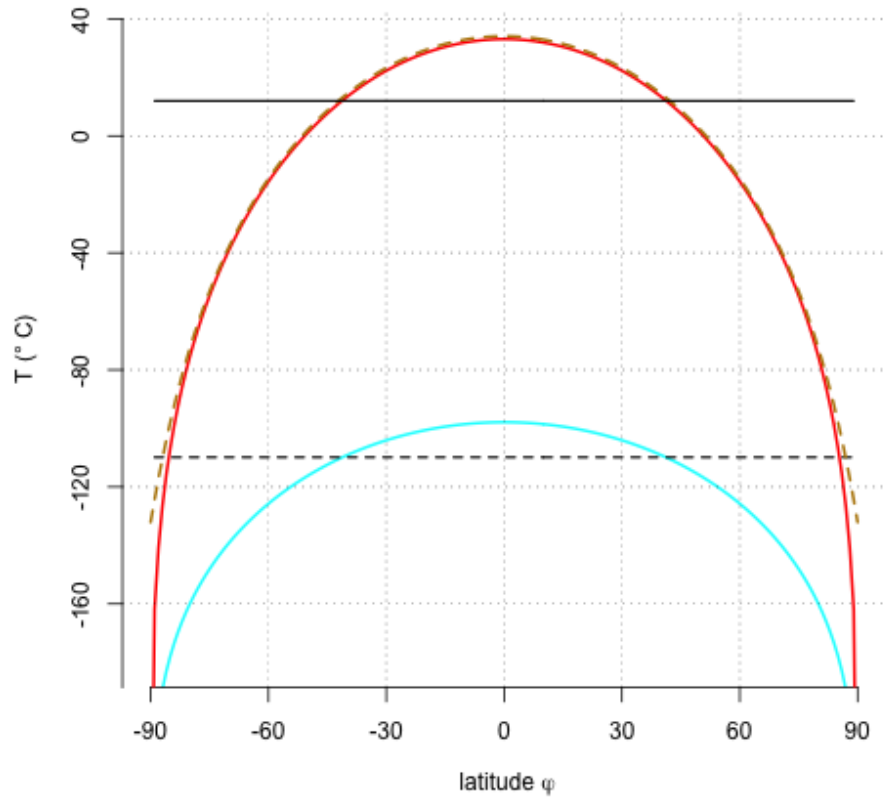
Figure 3. Latitudinal temperatures of the EBM with zero heat capacity (7) in cyan (its mean as a dashed line), the global approach (3) as solid black line, and the zonal and time averaging (11) in red. The dashed brownish curve shows the numerical solution by taking the zonal mean of (9).
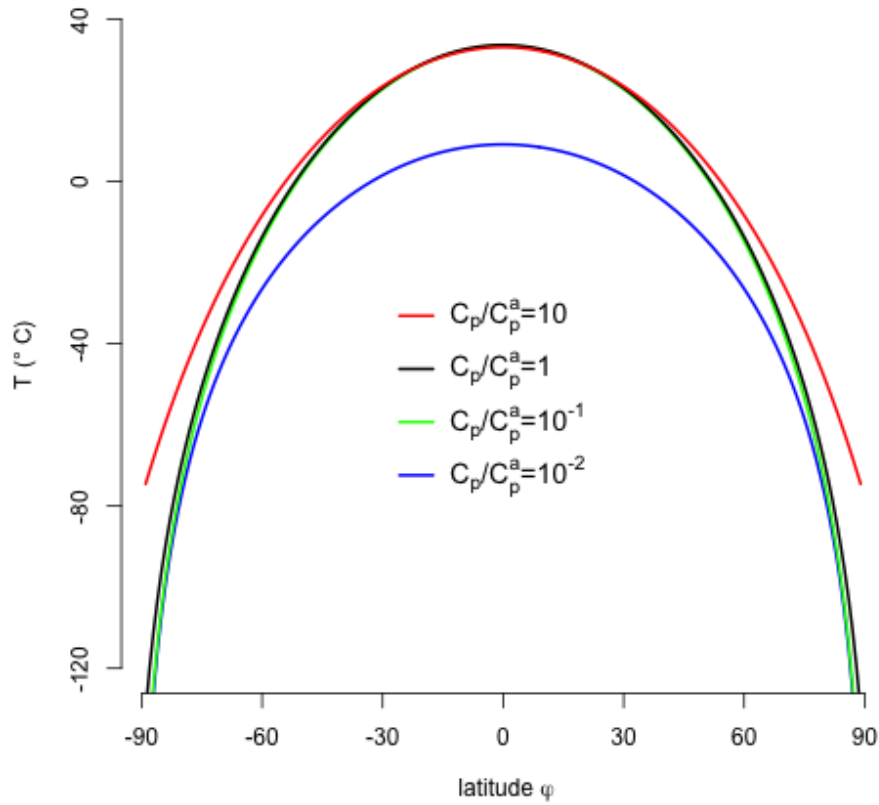
Figure 4. Temperature depending on C_p when solving (9) numerically. The reference heat capacity is the atmospheric heat capacity $C_p^a = 1.02 \cdot 10^7 \, JK^{-1}m^{-2}$. The climate is insensitive to changes in heat capacity $C_p \in [0.05 \cdot C_p^a, 2 \cdot C_p^a]$.
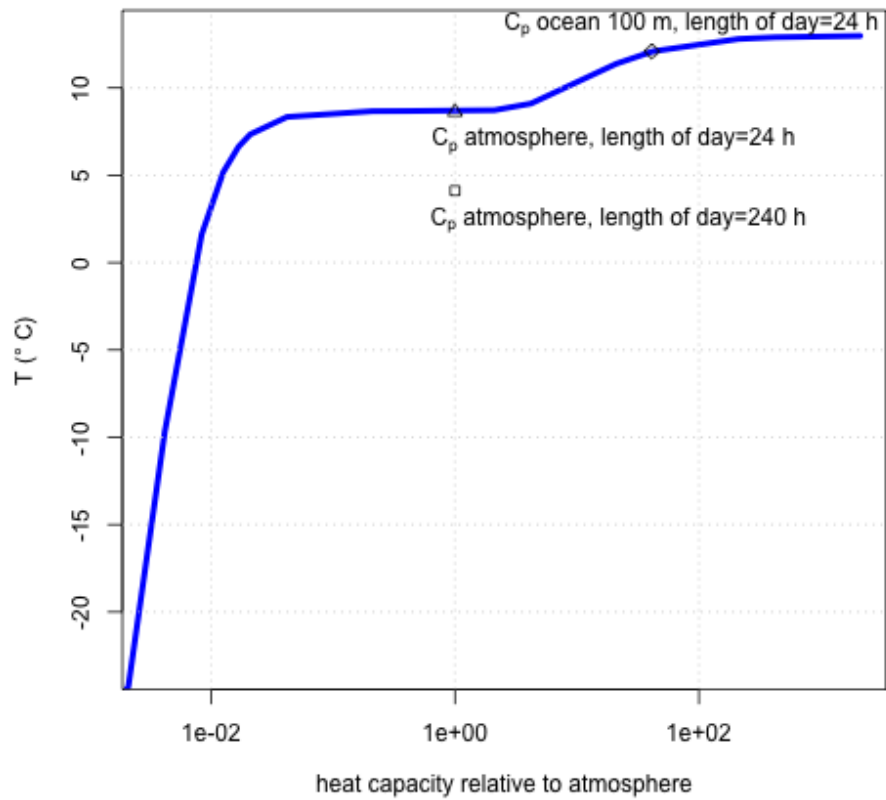
Figure 5. Temperature dependence on heat capacity (and rotation rate) when analyzing the daily mean temperature at 45°N using (9).
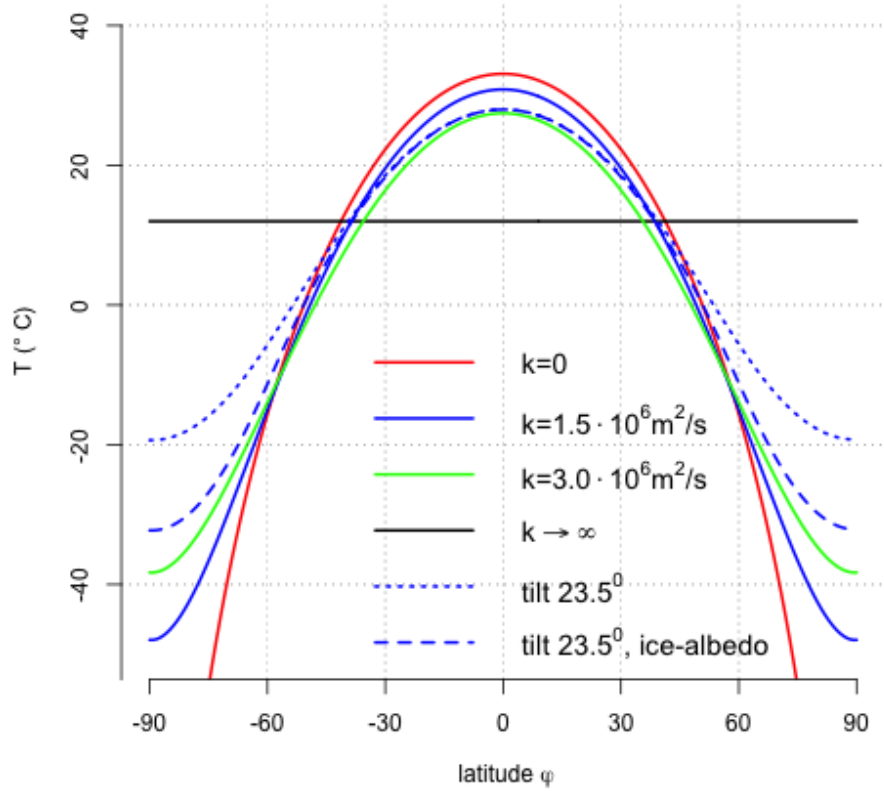
Figure 6. Equilibrium temperature of (13) using different diffusion coefficients. $C_p = C_p^a$. The blue lines use $1.5 \cdot 10^6 m^2/s$ with no tilt (solid line), a tilt of $23.5°$ (dotted line), and as the dashed line a tilt of $23.5°$ (present value) and ice-albedo feedback using the respresentation of Sellers (1969). Except for the dashed line, the global mean values are identical to the value calculated in (12). Units are °C.
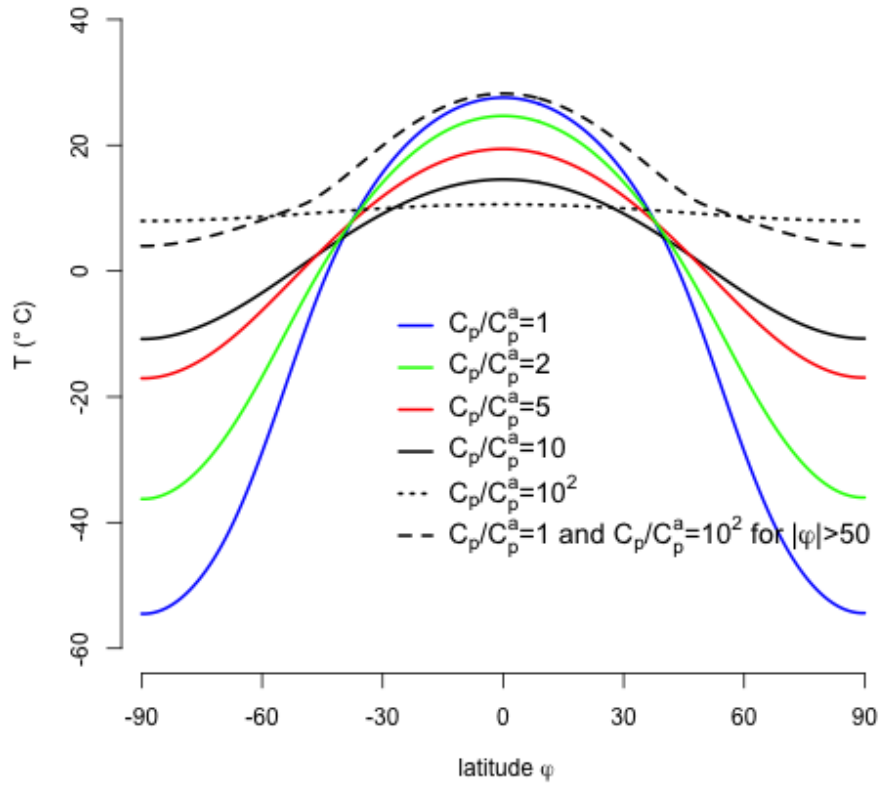
Figure 7. Annual mean temperature depending on C_p when solving the seasonal resolved EBM (14) numerically. For all solutions, we use use $k = 1.5 \cdot 10^6 m^2/s$, present day orbital parameters, and the ice-albedo feedback using the resprensentation of Sellers (1969).
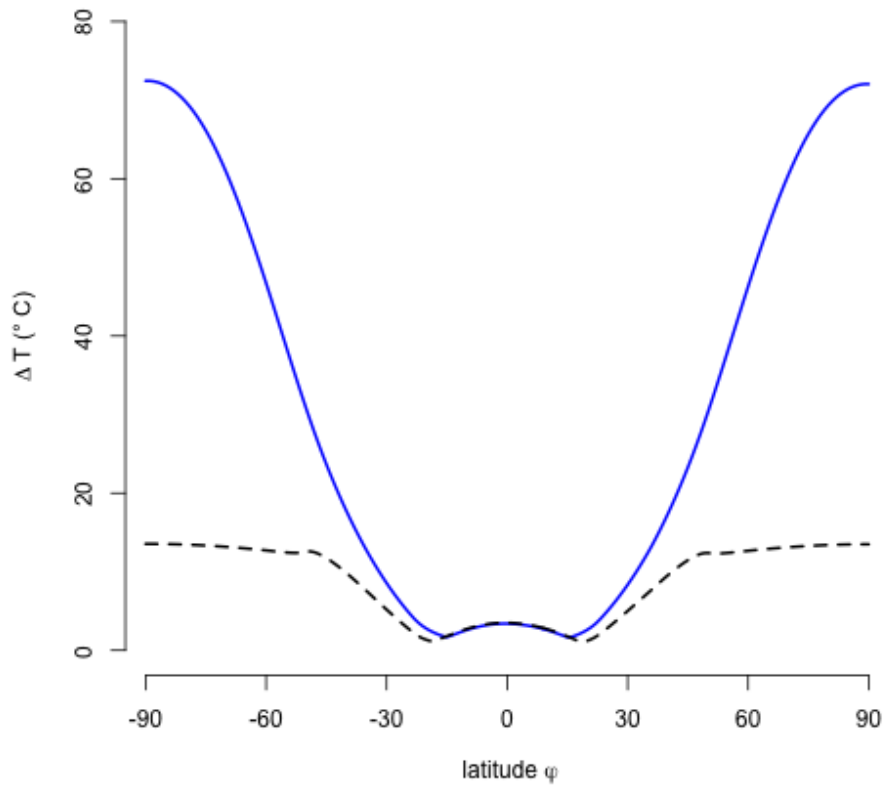
Figure 8. Seasonal amplitude of temperature for the two extreme scenarios in Fig. 7, indicating that a lower seasonality dashed-black relative to the blue line is linked to warmer annual mean climate.
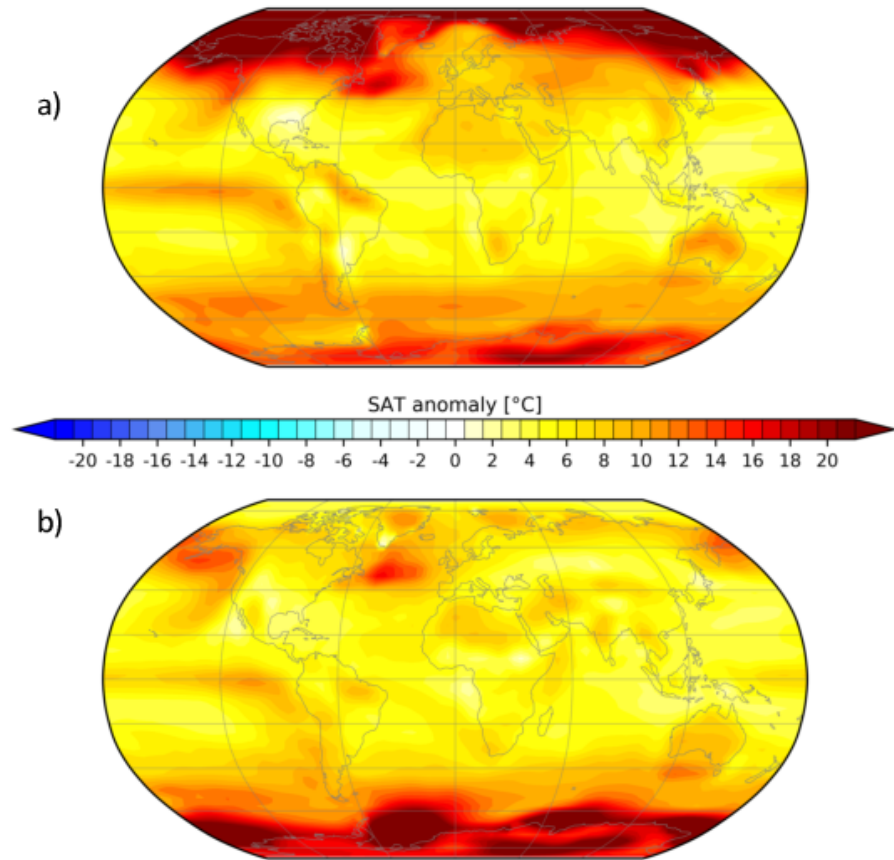
Figure 9. Anomalous near surface temperature for the vertical mixing experiment relative to the control climate. a) Mean over boreal winter and austral summer (DJF), b) Mean over austral winter and boreal summer (JJA). Shown is the 100 year mean after 900 years of integration using the Earth system model COSMOS. Units are °C.

References

Adem, J.: Experiments Aiming at Monthly and Seasonal Numerical Weather prediction. Mon. Weather Rev. 93,495-503, 1965.

Adem, J.: Numerical simulation of the annual cycle of climate during the ice ages, J. Geophys. Res., 86, 12015-12034, 1981.

Anderson S.P., Weller, R.A., and Lukas, R.B.: Surface buoyancy forcing and the mixed layer of the western pacific warm pool: observations and 1D model results. J. Clim. 9:3056-3085, 1996.

5   Archer, D.: Global Warming: Understanding the Forecast. ISBN: 978-1-4443-0899-0. 288 pages, Wiley-Blackwell, 2009.

Berger, A., and Loutre, M.F.: Insolation values for the climate of the last 10 million years, Quat. Sci. Rev., 10(4), 297 - 317, 1991.

Berger, A., and Loutre, M.F.: Intertropical latitudes and precessional and half-precessional cycles, Science, 278(5342), 1476 - 1478, 1997.

Budyko, M.I.: The effect of solar radiation variations on the climate of the Earth. Tellus 21,611-619, 1969.

Chen, D., Gerdes, R., and Lohmann, G.: A 1-D Atmospheric energy balance model developed for ocean modelling. Theor. Appl. Climatol.

10   51, 25-38, 1995.

Claussen, M., Mysak, L.A., Weaver, A.J., Crucifix, M., Fichefet, T., Loutre, M.-F., Weber, S.L., Alcamo, J.,Alexeev, V.A., Berger, A., Calov, R., Ganopolski, A., Goosse, H., Lohmann, G.,Lunkeit, F., Mokhov, I.I., Petoukhov, V., Stone, P., and Wang, Z.: Earth System Models of Intermediate Complexity: Closing the Gap in the Spectrum of Climate System Models. Climate Dynamics 18, 579-586, 2002.

de Boer, A. M. and Hogg, A. M.: Control of the glacial carbon budget by topographically induced mixing, Geophys. Res. Lett., 41, 4277-

15   4284, 2014.

de Boyer Montégut C., Gurvan M., and Fischer A. S.: Mixed layer depth over the global ocean: an examination of profile data and a profilebased climatology. Journal of Geophysical Research: Oceans, 109 (C12): C12003, 2004.

Donohoe A., Frierson D.M.W., and Battisti D.S.: The effect of ocean mixed layer depth on climate in slab ocean aqua-planet experiments. Clim. Dyn. 43(3-4):1041?1055, 2014.

20   Dowsett, H. J. , K. M. Foley, D. K. Stoll, M. A. Chandler, L. E. Sohl, M. Bentsen, B. L. Otto-Bliesner, F. J. Bragg, W.-L. Chan, C. Contoux, A. M. Dolan, A. M. Haywood, J. A. Jonas, A. Jost, Y. Kamae, G. Lohmann, D. J. Lunt , K. H. Nisancioglu, A. Abe-Ouchi, G. Ramstein, C. R. Riesselman, M. M. Robinson, N. A. Rosenbloom, U. Salzmann, C. Stepanek, S. L. Strother, H. Ueda, Q. Yan, Z. Zhang: Sea Surface Temperature of the mid-Piacenzian Ocean: A Data-Model Comparison. Scientific Reports 3; Article number: 2013; DOI:10.1038/srep02013, 2013.

25   Fanning, A.F., and Weaver, A. J.: An atmospheric energy-moisture balance model: Climatology, interpentadal climate change, and coupling to an ocean general circulation model. J. Geophys. Res. 101 (D10), 15111-15128, 1996.

Fu, R., Del Genio, A.D., and Rossow, W.B.: Influence of ocean surface conditions on atmospheric vertical thermodynamic structure and deep convection. J. Climate, 7, 1092-1107, 1994.

Ghil, M.: Climate stability for a Sellers-type model. J. Atmos. Sci., 33, 3-20, 1976.

30   Ghil, M, and Childress, S.: Topics in geophysical fluid dynamics: atmospheric dynamics, dynamo theory, and climate dynamics. New York, NY: Springer, 1987.

Green, J.A.M., and Huber, M.: Tidal dissipation in the early Eocene and implications for ocean mixing, Geophys. Res. Lett., 40, 2707?2713, doi:10.1002/grl.50510, 2013.

Griffies, S.M.: Fundamentals of Ocean Climate Models. Princeton University Press, Princeton, USA. ISBN9780691118925 528 pp, 2005.

35   Griffiths, S.D., and Peltier, W.R.: Modeling of Polar Ocean Tides at the Last Glacial Maximum: Amplification, Sensitivity, and Climatological Implications. J. Clim. 22, 2905-2924, 2009.

Goosse, H.: Climate system dynamics and modelling. Cambridge University Press, ISBN: 9781107445833, 2015.

Hansen, J., Ruedy, R., Sato, M., and Lo, K.: Global surface temperature change. Rev. Geophys., 48, RG4004, doi:10.1029/2010RG000345, 2010.

Hardy, G. H., Littlewood, J. E., Pólya, G.: Inequalities. 1934. Cambridge University Press, pp. 314, ISBN 0-521-35880-9, JFM 60.0169.01

Hartmann, D. L., Global Physical Climatology, Academic Press, 1994.

Hasselmann, K.: Stochastic climate models. Part I, Theory. Tellus, 6:473–485, 1976.

Hölder, O.: Ueber einen Mittelwertsatz. Nachrichten von der Königl. Gesellschaft der Wissenschaften und der Georg-Augusts-Universität zu Göttingen, 2, 38-47, 1889.

Huber, B.T., MacLeod, K.G., and Wing, S.L. (Eds.): Warm Climates in Earth History. Cambridge University Press, 462 pp, 2000.

Huber, M., H. Brinkhuis, C. E. Stickley, K. Doos, A. Sluijs, J. Warnaar, G. L. Williams, and S. A. Schellenberg: Eocene circulation of the Southern Ocean: Was Antarctica kept warm by subtropical waters?, Paleoceanography, 19, PA4026, doi:10.1029/2004PA001014, 2004.

Jungclaus, J. H., Lorenz, S. J., Timmreck, C., Reick, C. H., Brovkin, V., Six, K., Segschneider, J., Giorgetta, M. A., Crowley, T. J., Pongratz, J., Krivova, N. A., Vieira, L. E., Solanki, S. K., Klocke, D., Botzet, M., Esch, M., Gayler, V., Haak, H., Raddatz, T. J., Roeckner, E., Schnur, R., Widmann, H., Claussen, M., Stevens, B., and Marotzke, J.: Climate and carbon-cycle variability over the last millennium, Clim. Past, 6, 723-737, 2010.

Kawai, Y., and Kawamura, H.: Evaluation of the diurnal warming of sea surface temperature using satellite derived marine meteorological data. J Oceanogr 58:805-814, 2002.

Knorr, G., Butzin, M., Micheels, A., and Lohmann, G.: A Warm Miocene Climate at Low Atmospheric CO_2 levels. Geophysical Research Letters, L20701, doi:10.1029/2011GL048873, 2011.

Knorr, G., and Lohmann, G.: A warming climate during the Antarctic ice sheet growth at the Middle Miocene transition. Nature Geoscience, 7, 376-381, 2014.

Köhler, P., Bintanja, R., Fischer, H., Joos, F., Knutti, R., Lohmann, G., and Masson-Delmotte, V.: What caused Earth's temperature variations during the last 800,000 years? Data-based evidence on radiative forcing and constraints on climate sensitivity. Quaternary Science Reviews 29, 129-145. doi:10.1016/j.quascirev.2009.09.026, 2010.

Korty, R. L, Emanuel, A. K. A., and Scott, J. R.: Tropical Cyclone-Induced Upper-Ocean Mixing and Climate: Application to Equable Climates. J. Climate, 21, 638-654, 2008.

Kuptsov, L. P.: Hölder inequality. In Hazewinkel, Michiel (ed.), Encyclopedia of Mathematics, Springer Science+Business Media B.V. / Kluwer Academic Publishers, ISBN 978-1- 55608-010-4, 2001.

Laepple, T., and Lohmann, G.: The seasonal cycle as template for climate variability on astronomical time scales. Paleoceanography, 24, PA4201, doi:10.1029/2008PA001674, 2009.

Lambeck, K.: Tidal dissipation in the oceans: astronomical, geophysical and oceanographic consequences Phil. Trans. R. Soc. Lond. A, 287, 545-594, 1977.

Large, W.G., McWilliams, J.C., and Doney, S.C.: Oceanic vertical mixing: a review and a model with a nonlocal boundary layer parameterization Rev. Geophys., 32 (4), 363-403, 1994.

Lemke, P.: Stochastic climate models, part 3. Application to zonally averaged energy models, Tellus, 29:5, 385-392, 1977.

La Riviere, J.P., Ravelo, A.C., Crimmins, A., Dekens, P.S., Ford, H.L., Lyle, M., Wara, M.W.: Late Miocene decoupling of oceanic warmth and atmospheric carbon dioxide forcing. Nature 486, 97-100, 2012.

Le Treut, H., R. Somerville, U. Cubasch, Y. Ding, C. Mauritzen, A. Mokssit, T. Peterson and M. Prather: Historical Overview of Climate Change. In: Climate Change 2007: The Physical Science Basis. Contribution of Working Group I to the Fourth Assessment Report of the Intergovernmental Panel on Climate Change [Solomon, S., D. Qin, M. Manning, Z. Chen, M. Marquis, K.B. Averyt, M. Tignor and H.L. Miller (eds.)]. Cambridge University Press, Cambridge, United Kingdom and New York, NY, USA, 2007.

Lohmann, G.: ESD Ideas: The stochastic climate model shows that underestimated Holocene trends and variability represent two sides of the same coin. Earth Syst. Dynam. 9, 1279-1281, 2018.

Lohmann, G., Pfeiffer, M., Laepple, T., Leduc, G., and Kim, J.-H.: A model-data comparison of the Holocene global sea surface temperature evolution. Clim. Past, 9, 1807-1839, 2013.

Lohmann, G., Gerdes, R., and Chen, D.: Sensitivity of the thermohaline circulation in coupled oceanic GCM-atmospheric EBM experiments. Climate Dynamics 12, 403-416, 1996.

Lohmann, G., and Gerdes, R.: Sea ice effects on the Sensitivity of the Thermohaline Circulation in simplified atmosphere-ocean-sea ice models. J. Climate 11, 2789-2803, 1998.

Luyten, J., Pedlosky, J., and Stommel, H.: The ventilated thermocline. J. Phys. Oceanogr., 13, 292-309, 1983.

Markwick, P.J.: 'Equability', continentality and Tertiary 'climate': the crocodilian perspective. Geology, 22, 613-616, 1994.

Mosbrugger, V., Utescher, T. , and D. L. Dilcher: Cenozoic continental climatic evolution of Central Europe. Proceedings National Academy of Sciences, 102: 14964-14969, 2005.

Munk, W., and Wunsch, C.: Abyssal recipes II: Energetics of tidal and wind mixing. Deep-Sea Res., 45, 1977-2010, 1998.

Nilsson, J.: Energy flux from traveling hurricanes to the oceanic internal wave field. J. Phys. Oceanogr., 25, 558-573, 1995.

North, G. R.: Analytical solution of a simple climate model with diffusive heat transport. J. Atm. Sci. 32, 1300-1307, 1975a

North, G. R.: Theory of energy-balance climate models. J. Atm. Sci. 32, 2033-2043, 1997b.

North G.R., Cahalan R.F., Coakley J.A.: Energy balance climate models. Rev. Geophys. Space Phys. 19, 91-121, 1981.

North G.R., Mengel, J.G., Short D.A.: Simple energy balance model resolving the seasons and the continents: application to the astronomical theory of the ice ages. J. Geophys. Res. 88, 6576-6586, 1983.

North, G. R., and Kim, K.-Y.: Energy Balance Climate Models. Wiley, 2017. ISBN:9783527411320, DOI:10.1002/9783527698844

Olbers, D.J., Wenzel, M., and Willebrand, J.: The inference of North Atlantic circulation patterns from climatological hydrographic data. Rev. Geophys. 23(4), 313-356, 1985.

Pacanowski, R. C., and Philander, S. G. H.: Parameterization of Vertical Mixing in Numerical Models of Tropical Oceans. J. Phys. Oceanogr. 11, 83-89, 1981.

Peixoto, J. P., and Oort, A. H.: Physics of Climate, ISBN-13: 978-0883187128, ISBN-10: 0883187124, AIP Press, Springer Verlag, Berlin Heidelberg, New York, 1992.

Pfeiffer, M., and Lohmann, G.: Greenland Ice Sheet influence on Last Interglacial climate: global sensitivity studies performed with an atmosphere-ocean general circulation model, Clim. Past, 12, 1313-1338, 2016.

Pierrehumbert, R.T.: Principles of Planetary Climate. Cambridge University Press. Online ISBN: 9780511780783 DOI:10.1017/CBO9780511780783, 2010.

Qiao, F., Yuan, Y., Yang, Y., Zheng, Q., Xia, C., and Ma, J.: Wave-induced mixing in the upper ocean: Distribution and application to a global ocean circulation model Geophysical Research Letters 31 (11), https://doi.org/10.1029/2004GL019824, 2004.

Reichl, B.G., and Hallberg, R.: A simplified energetics based planetary boundary layer (ePBL) approach for ocean climate simulations. Ocean Modelling 132, 112-129, 2018.

Rogers, L. J.: An extension of a certain theorem in inequalities. Messenger of Mathematics, New Series, XVII (10): 145?150, 1888. JFM 20.0254.02

Ruddiman, W.F.: Earth's Climate: Past and Future. W H Freeman & Co, 354 pages, ISBN-13: 978-0716737414, 2001.

Saltzman, B.: Dynamical Paleoclimatology: Generalized Theory of Global Climate Change. ISBN-13: 978-0123971616, ISBN-10: 0123971616, 2001.

5   Schneider, E.K., Zhu, Z.: Sensitivity of the simulated annual cycle of sea surface temperature in the equatorial Pacific to sunlight penetration. J. Clim. 11, 1932-1950, 1998.

Schwartz, S.E.: Heat capacity, time constant, and sensitivity of Earth's climate system. J Geophys Res 112: D24S05, doi:10.1029/2007JD008746, 2007.

Sellers, W. D.: A global climate model based on the energy balance of the earth-atmosphere system. J. Appl. Meteorol. 8, 392-400, 1969.

10   Sellers, W. D.: A new global climate model. J. Appl. Meteorol. 12, 241-254, 1973.

Shellito, C. J., Sloan, L. C., and Huber, M.: Climate model sensitivity to atmospheric CO2 levels in the early-middle Paleogene. Palaeogeogr. Palaeoclimatol. Palaeoecol., 193, 113-123, 2003.

Short, D. A., J. G. Mengel, T. J. Crowley, W. T. Hyde, and G. R. North: Filtering of Milankovitch Cycles by Earth's Geography. Quaternary Research 35, 2, 157-173, 1991.

15   Simmons, H. L., Jayne, S. R., Laurent, L. C. S., and Weaver, A. J.: Tidally driven mixing in a numerical model of the ocean general circulation, Ocean Model., 6, 245-263, https://doi.org/10.1016/S1463-5003(03)00011-8, 2004.

Sloan, L. C., and Rea, D. K.: Atmospheric carbon dioxide and early Eocene climate: A general circulation modeling sensitivity study. Palaeogeogr. Palaeoclimatol. Palaeoecol., 119, 275-292, 1996.

Sloan, L.C., and Barron, E.J.: Equable climates during Earth history Geology, 18, 489-492, 1990.

20   Sloan, L.C., Huber, M., Crowley, T.J., Sewall, J.O., and Baum S.: Effect of sea surface temperature configuration on model simulations of equable climate in the early Eocene Palaeogeogr. Palaeoclimatol. Palaeoecol., 167, 321-335, 2001.

Spicer R.A., Herman, A.B., and Kennedy E.M.: The foliar physiognomic record of climatic conditions during dormancy: CLAMP and the cold month mean temperature J. Geol., 112, 685-702, 2004.

Stein, R., K. Fahl, M. Schreck, G. Knorr, F. Niessen, M. Forwick, C. Gebhardt, L. Jensen, M. Kaminski, A. Kopf, J. Matthiessen,
25   W. Jokat, and G. Lohmann: Evidence for ice-free summers in the late Miocene central Arctic Ocean. Nature comm. 7, 11148, doi:10.1038/ncomms11148, 2016.

Stepanek, C., and Lohmann, G.: Modelling mid-Pliocene climate with COSMOS. Geosci. Model Dev., 5, 1221-1243, 2012.

Stocker, T.: Introduction to Climate Modelling. 182 pp. Springer-Verlag Berlin Heidelberg. doi:10.1007/978-3-642-00773-6 ISBN 978-3-642-00773-6, 2011.

30   Stocker, T.F., Wright, D.G., and Mysak, L.A.: A zonally averaged, coupled ocean-atmosphere model for paleoclimate studies. J. Climate 5, 773-797, 1992.

Stommel, H., Saunders, K., Simmons, W., and Cooper, J.: Observation of the diurnal thermocline. Deep-Sea Res., 16, 269-284, 1969.

Stuart-Menteth, A.C., Robinson, I.S., and Challenor, P.G.: A global study of diurnal warming using satellite-derived sea surface temperature. J Geophys Res 108(C5):3155, 2003.

35   Su, Q.H., and Hsieh, D.Y.: Stability of the Budyko climate model. J. Atmos. Sci., 33, 2273-2275, 1976.

Tripati, A. K., Delaney, M. L., Zachos, J. C., Anderson, L. D. Kelly, D. C., and Elderfield, H.: Tropical sea-surface temperature reconstruction for the early Paleogene using Mg/Ca ratios of planktonic foraminifera. Paleoceanography, 18, 1101, 2003.

Utescher, T., and Mosbrugger, V.: Eocene vegetation patterns reconstructed from plant diversity - A global perspective. Palaeogeography, Palaeoclimatology, Palaeoecology 247, 243-271, 2007.

Valdes, P.J., Sellwood, B.W., and Price, G.D.: The concept of Cretaceous equability Palaeoclim.: Data Model., 1, 139-158, 1996.

Vasavada, A.R., Paige, D.A., and Wood, S.E.: Near-surface temperatures on Mercury and the Moon and the stability of polar ice deposits. Icarus 141, 179-93, 1999.

5 von Storch, H., Güss, G. S., and Heimann, M.: Das Klimasystem und seine Modellierung: eine Einführung. (in German) Springer-Verlag Berlin Heidelberg. 256pp. doi:10.1007/978-3-642-58528-9, 1999.

Wang, Z., Schneider, E. K., and Burls, N. J.: The sensitivity of climatological SST to slab ocean model thickness. Climate Dynamics, 1-15, 2019. http://doi.org/10.1007/s00382-019-04892-0

Ward, B.: Near-surface ocean temperature. J Geophys Res 111(C5):1-18. doi:10.1029/2004JC002689, 2006.

10 Wei, W., and Lohmann, G.: Simulated Atlantic Multidecadal Oscillation during the Holocene. J. Climate, 25, 6989-7002, 2012.

Wiebe, E.C., and Weaver, A. J.: On the sensitivity of global warming experiments to the parameterisation of sub-grid scale ocean mixing. Climate Dyn., 15, 875-893, 1999.

Wolfe, J.A.: Tertiary climatic changes at middle latitudes of western North America. Palaeogeography, Palaeoclimatology, Palaeoecology 108, 195-205, 1994.

15 Zachos, J.C., Dickens, G.R., and Zeebe, R.E.: An early Cenozoic perspective on greenhouse warming and carbon-cycle dynamics. Nature, 451, 279-283, 2008.

Zhang, X., Lohmann, G., Knorr, G., and Xu, X.: Different ocean states and transient characteristics in Last Glacial Maximum simulations and implications for deglaciation. Clim. Past, 9, 2319-2333, 2013.

Zhang, X., Lohmann, G., Knorr, G., and Purcell, C.: Abrupt glacial climate shifts controlled by ice sheet changes. Nature 512, 290-294,
20 2014.